LINEAR FINITE ELEMENTS MAY BE ONLY FIRST-ORDER POINTWISE ACCURATE ON ANISOTROPIC TRIANGULATIONS

NATALIA KOPTEVA

Abstract. We give a counterexample of an anisotropic triangulation on which the exact solution has a second-order error of linear interpolation, while the computed solution obtained using linear finite elements is only first-order pointwise accurate. Our example is given in the context of a singularly perturbed reaction-diffusion equation, whose exact solution exhibits a sharp boundary layer. Furthermore, we give a theoretical justification of the observed numerical phenomena using a finite-difference representation of the considered finite element methods. Both standard and lumped-mass cases are addressed.

1. Introduction

It appears that there is a perception in the finite-element community that the computed-solution error in the maximum norm is closely related to the corresponding interpolation error. While an almost best approximation property of finite-element solutions in the maximum norm has been rigourously proved (with a logarithmic factor in the case of linear elements) for some equations on quasi-uniform meshes [12, 13], there is no such result for strongly-anisotropic triangulations. Nevertheless, this perception is frequently considered a reasonable heuristic conjecture to be used in the anisotropic mesh adaptation [7, 6, 8, 4].

In this note we give a counterexample of an anisotropic triangulation on which

- the exact solution is in $C^\infty(\bar\Omega)$ and has a second-order pointwise error of linear interpolation $O(N^{-2})$,
- the computed solution obtained using linear finite elements is only first-order pointwise accurate, i.e. the pointwise error is as large as $O(N^{-1})$.

Here the maximum side length of mesh elements is $O(N^{-1})$ and the global number of mesh nodes does not exceed $O(N^2)$.

Our example is given in the context of singularly perturbed differential equations. Their solutions exhibit sharp boundary and interior layers, so locally anisotropic meshes (fine and anisotropic in layer regions and standard outside) are frequently employed in their numerical solution and, furthermore, have been shown to yield reliable numerical approximations in an efficient way (see, e.g., [5, 9, 14] and references in [10]).

Date: September 14, 2012 and, in revised form, October xx, 2012.

1991 *Mathematics Subject Classification.* Primary 65N15, 65N30, 65N50; Secondary 65N06.

Key words and phrases. Anisotropic triangulation, linear finite elements, maximum norm, singular perturbation, Bakhvalov mesh, Shishkin mesh.

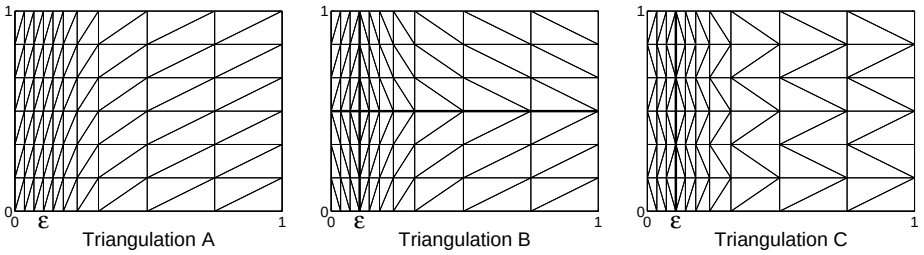

FIGURE 1. *Triangulations A, B and C are obtained from the same layer-adapted tensor-product mesh by drawing diagonals in a different manner. The bold lines indicate a change in the type of triangulation.*

Example. Consider an exact solution $u(x,y) = e^{-x/\varepsilon}$ of the singularly perturbed reaction-diffusion problem

$$-\varepsilon^2\Delta u + u = 0 \quad \text{for } (x,y) \in \Omega, \qquad u = g \quad \text{for } (x,y) \in \partial\Omega, \tag{1.1}$$

where ε is a small positive parameter, $\Delta = \partial^2/\partial x^2 + \partial^2/\partial y^2$ is the Laplace operator, and the boundary data g matches the chosen exact solution. The domain Ω is a bounded polygonal domain. In particular we consider the cases of $\Omega = (0,1)^2$ and $\Omega = (0,2\varepsilon)\times(0,1)$, as well as a more general case of $\Omega \supset \mathring{\Omega} := (0,2\varepsilon)\times(-H,H)$, where $H = O(N^{-1})$.

The paper is organized as follows. In §2, problem (1.1) is solved numerically using both standard and lumped-mass linear finite elements. Triangulations of types A, B and C are considered that are obtained from standard layer-adapted tensor-product meshes by drawing diagonals as on Figure 1. In §3, we give a theoretical justification of the observed numerical phenomena using a finite-difference representation of the considered finite element methods.

Notation. We let C denote a generic positive constant that may take different values in different formulas, but is always independent of the mesh and ε. A subscripted C (e.g., C_1) denotes a positive constant that is independent of N and ε and takes a fixed value. Notation $v = O(w)$ will be used for $C^{-1}w \le v \le Cw$, while $v = \mathcal{O}(w)$ will denote $|v| \le Cw$, with some constant C.

2. Numerical Results

Consider a tensor-product of a layer-adapted mesh $\{x_i\}_{i=0}^N$ in the x-direction and the uniform mesh $\{\frac{j}{M}\}_{j=0}^M$ in the y-direction, where $M = O(N)$. Whenever $\Omega = (0,1)^2$, the mesh $\{x_i\}$ will be a version of the Bakhvalov mesh [2] or the Shishkin mesh [14] described below. Whenever $\Omega = (0,2\varepsilon)\times(0,1)$, the mesh $\{x_i\}$ will be uniform.

Bakhvalov mesh [2] For some $\gamma \in (0,1)$, set $\sigma := 2\varepsilon(\gamma^{-1}|\ln\varepsilon| + 1)$ and assume that ε is sufficiently small for $\sigma \in (0,1)$. Now define the mesh $\{x_i\}_{i=0}^{N/2}$ on $[0,\sigma]$ by

$$x_i := x\big([1+\gamma-\varepsilon]\,\tfrac{2i}{N}\big), \quad x(t) := \begin{cases} 2\varepsilon\,\gamma^{-1}t, & t \in [0,\gamma] \\ 2\varepsilon\,[1-\gamma^{-1}\ln(1+\gamma-t)], & t \in [\gamma, 1+\gamma-\varepsilon] \end{cases}.$$

The remaining part of the mesh $\{x_i\}_{i=N/2}^N$ on $[\sigma,1]$ is uniform. In fact, one can easily see that on $[0,2\varepsilon]$ this mesh is also uniform, with $x_i - x_{i-1} = O(\varepsilon N^{-1})$.

TABLE 1. Bakhvalov tensor-product mesh, $\gamma = 0.8$, $M = \frac{1}{4}N$: maximum nodal errors and computational rates r in $(N^{-1})^r$.

		Triangulation A			Triangulation B		
	N	$\varepsilon = 2^{-8}$	$\varepsilon = 2^{-16}$	$\varepsilon = 2^{-24}$	$\varepsilon = 2^{-8}$	$\varepsilon = 2^{-16}$	$\varepsilon = 2^{-24}$
Lumped Masses	32	1.065e-3	1.070e-3	1.070e-3	1.543e-2	1.545e-2	1.545e-2
		1.99	1.99	1.99	1.07	1.07	1.07
	64	2.685e-4	2.697e-4	2.697e-4	7.328e-3	7.353e-3	7.353e-3
		2.00	2.00	2.00	0.98	0.97	0.97
	128	6.726e-5	6.756e-5	6.756e-5	3.713e-3	3.757e-3	3.757e-3
		2.00	2.00	2.00	1.03	0.99	0.99
	256	1.684e-5	1.691e-5	1.691e-5	1.818e-3	1.897e-3	1.897e-3
No Mass Lumping	32	1.422e-3	1.430e-3	1.430e-3	1.718e-2	1.723e-2	1.723e-2
		2.01	2.01	2.01	0.97	0.97	0.97
	64	3.526e-4	3.554e-4	3.554e-4	8.754e-3	8.811e-3	8.811e-3
		2.02	2.00	2.00	0.98	0.96	0.96
	128	8.710e-5	8.873e-5	8.873e-5	4.443e-3	4.527e-3	4.527e-3
		2.05	2.00	2.00	1.04	0.98	0.98
	256	2.097e-5	2.217e-5	2.217e-5	2.156e-3	2.292e-3	2.292e-3

Shishkin mesh [14] For some $\gamma \in (0,1)$, set $\sigma = 2\gamma^{-1}\varepsilon \ln \frac{N}{2}$. Now construct a piecewise-uniform mesh by dividing the intervals $[0,\sigma]$ and $[\sigma,1]$ into N_1 and $N-N_1$ equal subintervals for some $N_1 = O(N)$.

Remark 2.1 (Interpolation error). A calculation shows that the linear interpolation error of our exact solution $u = e^{-x/\varepsilon}$ on any of the Triangulations A, B or C is $O\big([N^{-1}\ln^p \frac{N}{2}]^2\big)$ in the maximum norm, where $p = 0$ if the Bakhvalov mesh is used or the uniform mesh in the domain $\Omega = (0, 2\varepsilon) \times (0,1)$, and $p = 1$ if the Shishkin mesh is used. Interestingly, one gets a similar second-order bound (with a logarithmic factor in the case of the Shishkin mesh) for the error of the standard five-point difference scheme applied to problem (1.1) on the corresponding tensor-product mesh (see, e.g., [5, 9]).

Tables 1–3 give the maximum nodal errors (odd rows) and the computational convergence rates r in $\big(N^{-1}\ln^p \frac{N}{2}\big)^r$ (even rows) for Triangulations A and B obtained from the three tensor-product meshes. For the considered values of ε, these meshes are highly anisotropic; for example, in the case of the Bakhvalov mesh (see Table 1), the mesh aspect ratio changes between 2 away from the layer and $(2.25\,\varepsilon)^{-1}$ in the layer region. The numerical results for the standard finite elements are quite similar to the case of mass lumping, so we consider both cases only in Table 1.

We observe that whenever Triangulation A is used, one gets a second-order accuracy, with a logarithmic factor in the case of the Shishkin mesh (similar to the accuracy of the five-point finite-difference scheme, which, in fact, is identical with the lumped-mass finite elements on Triangulation A). However, when one switches to Triangulation B, linear finite elements become only (almost) first-order pointwise accurate in contrast to the (almost) second-order accuracy of the interpolation error. Triangulation C also yields only (almost) first-order convergence (see also Remark 3.6 and Figure 3).

TABLE 2. Shishkin mesh, $\gamma = 0.9$, $M = \frac{1}{4}N$, $N_1 = \frac{3}{4}N$: maximum nodal errors and computational rates r in $(N^{-1} \ln \frac{N}{2})^r$

		Triangulation A			Triangulation B		
	N	$\varepsilon = 2^{-8}$	$\varepsilon = 2^{-16}$	$\varepsilon = 2^{-24}$	$\varepsilon = 2^{-8}$	$\varepsilon = 2^{-16}$	$\varepsilon = 2^{-24}$
Lumped Masses	32	1.850e-3	2.109e-3	2.109e-3	1.477e-2	1.478e-2	1.478e-2
		3.30	3.28	3.28	1.22	1.22	1.22
	64	3.930e-4	4.516e-4	4.521e-4	8.317e-3	8.340e-3	8.340e-3
		2.00	2.27	2.27	0.98	0.96	0.96
	128	1.418e-4	1.418e-4	1.418e-4	5.048e-3	5.103e-3	5.103e-3
		2.00	2.00	2.00	1.02	0.97	0.97
	256	4.832e-5	4.832e-5	4.832e-5	2.908e-3	3.027e-3	3.027e-3

TABLE 3. Uniform mesh in $(0, 2\varepsilon) \times (0, 1)$, $M = \frac{1}{4}N$: maximum nodal errors and computational rates r in $(N^{-1})^r$

		Triangulation A			Triangulation B		
	N	$\varepsilon = 2^{-8}$	$\varepsilon = 2^{-16}$	$\varepsilon = 2^{-24}$	$\varepsilon = 2^{-8}$	$\varepsilon = 2^{-16}$	$\varepsilon = 2^{-24}$
Lumped Masses	32	4.767e-5	4.767e-5	4.767e-5	2.985e-3	2.986e-3	2.986e-3
		2.00	2.00	2.00	1.02	1.02	1.02
	64	1.193e-5	1.193e-5	1.193e-5	1.474e-3	1.476e-3	1.476e-3
		2.00	2.00	2.00	1.02	1.01	1.01
	128	2.983e-6	2.983e-6	2.983e-6	7.288e-4	7.339e-4	7.339e-4
		2.00	2.00	2.00	1.03	1.00	1.00
	256	7.458e-7	7.458e-7	7.458e-7	3.561e-4	3.659e-4	3.659e-4

In summary, we conclude that

- when Triangulations B and C are used, linear finite elements are only first-order pointwise accurate;
- the order of convergence dramatically deteriorates from 2 to 1 as one switches from Triangulation A to Triangulation B or C.

Remark 2.2 (Comparison with the L_2 projection error). The L_2 projection errors are less understood on general anisotropic meshes. But one can easily estimate the pointwise error of this projection for the triangulations addressed in Table 3, i.e. obtained from the uniform tensor-product mesh in the domain $(0, 2\varepsilon) \times (0, 1)$. Indeed, the stretching transformation $\hat{x} := x/\varepsilon$ maps any of Triangulations A, B or C of the domain $(0, 2\varepsilon) \times (0, 1)$ into a quasi-uniform triangulation in the domain $(0, 2) \times (0, 1)$. Denoting the L_2 projection operators on the original and stretched triangulations by P and $\hat{P}$, respectively, one gets $Pu(x, y) = \hat{P}u(\varepsilon\hat{x}, y)$. As on the quasi-uniform stretched triangulation $\hat{P}u(\varepsilon\hat{x}, y) - u(\varepsilon\hat{x}, y) = \mathcal{O}(N^{-2})$, the L_2 projection error bound $Pu(x, y) - u(x, y) = \mathcal{O}(N^{-2})$ follows. So in this case, the exact solution has a second-order pointwise error of the L_2 projection, while, as Table 3 demonstrates, the pointwise error of the computed solution obtained using linear finite elements may be only first-order pointwise accurate.

TABLE 4. Normalized L_2 norm errors $\varepsilon^{-1/2}\|U-u^I\|_{L_2(\Omega)}$ and computational rates r in $(N^{-1})^r$: Bakhvalov tensor-product mesh, $\gamma=0.8$, $M=\frac{1}{4}N$

		Triangulation A		Triangulation B		Triangulation C	
	N	$\varepsilon=2^{-16}$	$\varepsilon=2^{-24}$	$\varepsilon=2^{-16}$	$\varepsilon=2^{-24}$	$\varepsilon=2^{-16}$	$\varepsilon=2^{-24}$
Lumped Masses	32	1.660e-3	2.000e-3	4.551e-3	4.679e-3	7.985e-3	8.058e-3
		2.14	2.22	1.62	1.65	1.05	1.06
	64	3.775e-4	4.300e-4	1.478e-3	1.492e-3	3.861e-3	3.866e-3
		2.09	2.16	1.51	1.52	0.96	0.96
	128	8.874e-5	9.618e-5	5.179e-4	5.192e-4	1.988e-3	1.989e-3
		2.05	2.10	1.51	1.51	0.98	0.98
	256	2.148e-5	2.247e-5	1.823e-4	1.824e-4	1.010e-3	1.010e-3

Errors in the L_2 norm. Although our main interest in this paper is in the pointwise accuracy of computed solutions, in Table 4 we also list the normalized L_2 norm errors $\varepsilon^{-1/2}\|U-u^I\|_{L_2(\Omega)}$ (odd rows) and the computational convergence rates r in $(N^{-1})^r$, where u^I is the piecewise-linear interpolant of u, for the Bakhvalov mesh. The table suggests that $\|U-u^I\|_{L_2(\Omega)}\approx O(\sqrt{\varepsilon}\,N^{-q})$, where q is 2, $\frac{3}{2}$ and 1 for Triangulations A, B and C, respectively. Thus although Triangulations B and C yield very similar maximum nodal errors, the latter is superior when the errors are computed in the L_2 norm (see also Figure 3, and Remark 3.6 for a theoretical explanation). The numerical results for the standard finite elements are quite similar to the case of mass lumping, so not presented here.

When we switch to the uniform tensor-product mesh in the domain $(0,2\varepsilon)\times(0,1)$ (as used in Table 3) to obtain triangulations of type A, B and C, the numerical results again suggest that $\|U-u^I\|_{L_2(\Omega)}\approx O(\sqrt{\varepsilon}\,N^{-q})$. Finally, for the Shishkin mesh (as used in Table 2), one computationally observes that $\|U-u^I\|_{L_2(\Omega_\sigma)}\approx O\big(\sqrt{\varepsilon}\,N^{-q}[\ln\frac{N}{2}]^{\max\{1,2q-2\}}\big)$, where $\Omega_\sigma:=(0,\sigma)\times(0,1)$ is essentially the boundary-layer region (while the $L_2(\Omega\backslash\Omega_\sigma)$ norm of the error is quite small ε-independently).

It should also be noted that these results are obtained for the exact solution $e^{-x/\varepsilon}$, which is negligible away from the boundary-layer region. In general, the errors in the L_2 norm may involve an additional component $\mathcal{O}(N^{-2})$ induced by a nontrivial smooth part of the exact solution.

3. Theoretical Justification

To understand the numerical phenomena described in the previous section, we represent the considered finite elements as finite-difference schemes on the underlying rectangular tensor-product meshes.

Suppose $\Omega\supset\mathring{\Omega}$, where the subdomain $\mathring{\Omega}$ and the tensor-product mesh $\mathring{\omega}_h$ in this subdomain are defined by

$$\mathring{\Omega}:=(0,2\varepsilon)\times(-H,H),\quad \mathring{\omega}_h:=\{x_i=hi\}_{i=0}^{2N_0}\times\{-H,0,H\},\quad h=\tfrac{\varepsilon}{N_0}. \tag{3.1}$$

The triangulation $\mathring{\mathcal{T}}$ in $\mathring{\Omega}$ is obtained by drawing diagonals in each rectangle as shown on Figure 2, using the mesh transition point $(\varepsilon,0)$.

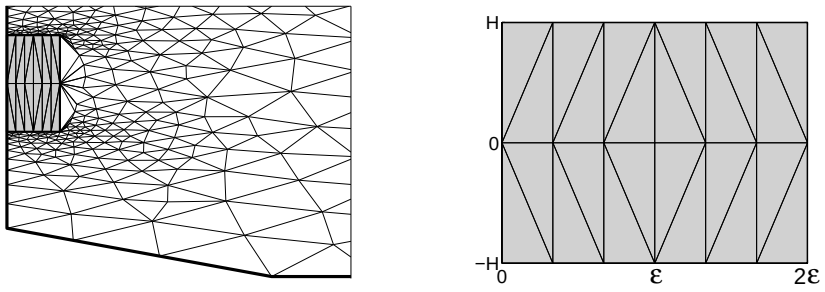

FIGURE 2. *Triangulation in Ω; right-hand picture enlarges the subdomain $\mathring{\Omega}$.*

Next, let U be the piecewise-linear finite-element solution obtained on some triangulation $\mathcal{T} \supset \mathring{\mathcal{T}}$ in the global domain Ω, for whose nodal values in $\mathring{\Omega}$ we use the notation

$$U_i := U(x_i, 0), \qquad U_i^{\pm} := U(x_i, \pm H).$$

Now a calculation yields a finite-difference representation in the *lumped-mass* case:

$$\mathcal{L}^h U(x_i,0) := \tfrac{\varepsilon^2}{h^2}[-U_{i-1} + 2U_i - U_{i+1}] + \tfrac{\varepsilon^2}{H^2}[-U_i^- + 2U_i - U_i^+] + \gamma_i U_i = 0 \tag{3.2a}$$

for $i = 1, \dots, 2N_0 - 1$, where

$$\gamma_i = 1 \quad \text{for } i \neq N_0, \qquad \gamma_{N_0} = \tfrac{2}{3}. \tag{3.2b}$$

In the *standard (non-lumped-mass)* case, one gets a similar finite-difference representation for $i = 1, \dots, 2N_0 - 1$:

$$\tilde{\mathcal{L}}^h U(x_i,0) := \mathcal{L}^h U_i - \tfrac{1}{12} \sum_{(x',y') \in \mathcal{S}_i} [U_i - U(x',y')] = 0, \tag{3.3}$$

where $\mathcal{S}_i$ denotes the set of meshnodes that have a common edge with $(x_i, 0)$.

Remark 3.1. Note that if γ_i in (3.2a) is replaced by 1, one gets the standard five-point difference scheme for equation (1.1), for which, using the discrete maximum principle, one can easily show that if a tensor-product mesh of type $\mathring{\omega}_h$ is used in the entire domain Ω, then the nodal error is $O\big(\frac{h^2}{\varepsilon^2}\big)$. Our method differs from this difference scheme at one point $(x_{N_0}, 0)$, where $\gamma_i = \frac{2}{3}$, i.e. at this point, compared to the second-order finite-difference method, we have a truncation error $O(1)$. As we show in Lemma 3.3 below, this results in the deterioration of pointwise accuracy of the computed solution to $O\big(\frac{h}{\varepsilon}\big)$.

Remark 3.2. A triangulation, similar to Triangulation B on Figure 1 (and also to triangulation $\mathring{\mathcal{T}}$ on Figure 2 (right)), but obtained from a uniform tensor-product mesh, has been used to show that the logarithmic factor in the L_∞-norm error estimate for linear finite elements applied to the Laplace equation is sharp [3, 1]. Our approach is, in fact, similar to that in [1] in that we represent a finite element method as a finite-difference scheme to get a lower bound for the error.

We shall consider the lumped-mass and non-lumped-mass cases separately.

3.1. **Lumped-Mass Linear Finite Elements.**

Lemma 3.3 (Lumped-mass case)**.** *Let $u = e^{-x/\varepsilon}$ be the exact solution of problem (1.1) posed in a domain $\Omega \supset \mathring{\Omega}$, a triangulation $\mathcal{T}$ in Ω be such that $\mathcal{T} \supset \mathring{\mathcal{T}}$ subject to the definitions (3.1), and U be the computed solution obtained using lumped-mass linear finite elements. For any positive constant C_2, there exist sufficiently small constants C_0 and C_1 such that if $N_0^{-1} \le C_1$ and $\varepsilon \le C_2 H$, then*

$$\max_{\bar{\Omega}} |U - u| \ge C_0 N_0^{-1}. \tag{3.4}$$

Proof. (i) First, consider the auxiliary piecewise-linear computed solution $\mathring{U}$ obtained on the triangulation $\mathring{\mathcal{T}}$ in the subdomain $\mathring{\Omega}$, subject to the boundary conditions $\mathring{U}(x', y') = u(x', y')$ at each meshnode $(x', y') \in \partial\mathring{\Omega}$. At the interior meshnodes, $\mathring{U}$ satisfies (3.2a), i.e. $\mathcal{L}^h \mathring{U}(x_i, 0) = 0$ for $i = 1, \dots, 2N_0 - 1$. We shall now prove that, for a sufficiently small constant C_0, one has

$$[\mathring{U} - u](x_{N_0}, 0) \ge 2C_0 N_0^{-1}. \tag{3.5}$$

Let $e := \mathring{U} - u$ and $e_i := e(x_i, 0)$. Recall that $e(x_i, \pm H) = 0$, so $\mathcal{L}^h e(x_i, 0)$ can be rewritten using a one-dimensional discrete operator L_x^h applied the unknown vector $\{e_i\}_{i=0}^{2N_0}$ as

$$\mathcal{L}^h e(x_i, 0) = L_x^h e_i := \tfrac{\varepsilon^2}{h^2}[-e_{i-1} + 2e_i - e_{i+1}] + \big[\gamma_i + \tfrac{2\varepsilon^2}{H^2}\big] e_i. \tag{3.6}$$

On the other hand, $\mathcal{L}^h e(x_i, 0) = -\mathcal{L}^h u(x_i, 0)$, so the standard truncation error estimation (using $u(x_i, \pm H) = u(x_i, 0)$) yields

$$\mathcal{L}^h e(x_i, 0) = [1 - \gamma_i]\, u(x_i, 0) + \mathcal{O}\big(\tfrac{h^2}{\varepsilon^2}\big). \tag{3.7}$$

Here, by virtue of (3.2b), $[1 - \gamma_i]u(x_i, 0) = [\frac{1}{3}\delta_{iN_0}]e^{-x_i/\varepsilon} = \frac{1}{3}e^{-1}\delta_{iN_0}$, where δ_{iN_0} denotes the Kronecker delta. So combining (3.6) and (3.7) yields

$$L_x^h e_i = \tfrac{1}{3}e^{-1}\delta_{iN_0} + \mathcal{O}\big(\tfrac{h^2}{\varepsilon^2}\big).$$

As L_x^h satisfies the discrete maximum principle [11], one gets the representation

$$[\mathring{U} - u](x_i, 0) = e_i = \tfrac{1}{3}e^{-1} h\, G_i^h + \mathcal{O}\big(\tfrac{h^2}{\varepsilon^2}\big). \tag{3.8}$$

Here G_i^h is the discrete Green's function of the one-dimensional operator L_x^h that satisfies $L_x^h G_i^h = h^{-1}\delta_{iN_0}$ for $i = 1, \dots, 2N_0 - 1$, subject to $G_0^h = G_{2N_0}^h = 0$. To complete the proof of (3.5), it now suffices to show that $G_{N_0}^h \ge C_3 \varepsilon^{-1}$ for some constant C_3; then one simply needs to choose sufficiently small constants C_0 and C_1 such that $\frac{1}{3}e^{-1}C_3\frac{h}{\varepsilon} + \mathcal{O}\big(\frac{h^2}{\varepsilon^2}\big) \ge 2C_0\frac{h}{\varepsilon}$. (To be more precise, $C_0 := \frac{1}{12}e^{-1}C_3$, while, by virtue of $\frac{h}{\varepsilon} = N_0^{-1} \le C_1$, we choose C_1 such that $\big|\mathcal{O}\big(\frac{h^2}{\varepsilon^2}\big)\big| \le \frac{1}{3}e^{-1}C_3\frac{h}{\varepsilon}$.)

To bound $G_{N_0}^h$, note that $G_i^h = G_{2N_0-i}^h$ and $G_i^h = G_{N_0}^h[w(x_i/\varepsilon) + \mathcal{O}(\frac{h^2}{\varepsilon^2})]$ for $i \le N_0$, where $w(x)$ solves the equation $-w'' + \big(1 + \frac{2\varepsilon^2}{H^2}\big)w = 0$ subject to $w(0) = 0$ and $w(1) = 1$. This implies that $\rho := \frac{\varepsilon}{h}[G_{N_0}^h - G_{N_0\pm1}^h]/G_{N_0}^h \le C_4$ for some constant $C_4 = C_4(C_2)$. (Roughly speaking, $\rho \approx w'(1) \le 1.32\sqrt{1 + 2C_2^2}$.) Now, $L_x^h G_{N_0}^h = h^{-1}$ can be rewritten as $G_{N_0}^h[2\frac{\varepsilon}{h}\rho + \big(\frac{2}{3} + \frac{2\varepsilon^2}{H^2}\big)\big] = h^{-1}$ or, equivalently, $G_{N_0}^h\big[2\rho + O\big(\frac{h}{\varepsilon}\big)\big] = \varepsilon^{-1}$. As $\frac{h}{\varepsilon} \le C_1$ and $\rho \ge C_4$, choosing C_1 sufficiently small we get $G_{N_0}^h \ge C_3\varepsilon^{-1}$ with $C_3 := (3C_4)^{-1}$, and, hence, the desired bound (3.5).

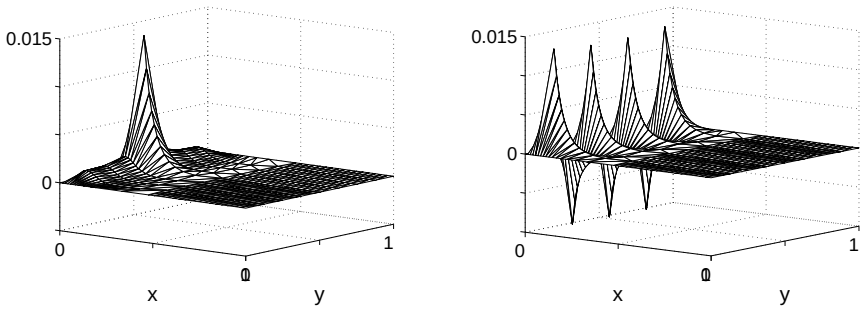

FIGURE 3. *Pointwise computed-solution error on Triangulation B (left) and C (right), Bakhvalov tensor-product mesh,* $\varepsilon = 0.05$*,* $N = 32$*,* $M = \frac{1}{4}N$*,* $\gamma = 0.8$.

(ii) In view of (3.5), to establish (3.4), it suffices to show that

$$\max_{\bar\Omega} |U - u^I| \ge \tfrac{1}{2} \max_{\mathring\Omega} |\mathring U - u^I| =: \tfrac{1}{2}\mathring e, \tag{3.9}$$

where u^I is the standard piecewise-linear interpolant of u.

Let $Z := U - \mathring U$ in $\mathring\Omega$ and $Z_{\max} := \sup_{\mathring\Omega} |Z|$. Note that $\mathcal{L}^h Z(x_i, 0) = 0$ and $Z = U - u^I$ on $\partial\mathring\Omega$. As, by the discrete maximum principle, $|Z|$ attains its maximum on $\partial\mathring\Omega$, so $\max_{\partial\mathring\Omega} |U - u^I| = Z_{\max}$. On the other hand, $U - u^I = (\mathring U - u^I) + Z$ yields $\max_{\mathring\Omega} |U - u^I| \ge \mathring e - Z_{\max}$ As the maximum of the two values $\mathring e - Z_{\max}$ and $Z_{\max}$ exceeds their average, the desired relation (3.9) follows. □

Remark 3.4. An inspection of the proof of Lemma 3.3 shows that if the assumption $\varepsilon \le C_2 H$ is replaced by a weaker $h \ll H$, one gets a version of (3.4) with C_0 replaced by $C_0'/\sqrt{1 + 2\frac{\varepsilon^2}{H^2}}$.

Remark 3.5. Lemma 3.3 applies to all triangulations of type B used in Tables 1–3, with $N_0^{-1} = O(N^{-1} \ln^p \frac{N}{2})$, where $p = 0$ if the Bakhvalov mesh is used or the uniform mesh in the domain $\Omega = (0, 2\varepsilon) \times (0, 1)$, and $p = 1$ if the Shishkin mesh is used. Furthermore, this lemma still applies if one switches from Triangulation B to Triangulation C.

Remark 3.6. For all triangulations considered in Section 2, one has $\varepsilon \ll M^{-1}$. So a version of part (i) of the proof of Lemma 3.3 (with negligible $\frac{\varepsilon^2}{H^2}$) can be applied to the global Triangulation B in Ω to show that $|[U-u](x,y)| \le C(N^{-1} \ln^p \frac{N}{2})^2$ whenever $|y - \frac{1}{2}| \ge M^{-1}$, i.e. the deterioration in the accuracy occurs only near $y = \frac{1}{2}$; see Figure 3 (left). However, if one switches to Triangulation C, a similar analysis yields $[U-u](x_i, \frac{j}{M}) = (-1)^j e_i$ with e_i from (3.8) and a slightly different G_i^h (now associated with the mesh $\{x_i\}_{i=0}^N$). Again, $\max e_i = O(N_0^{-1}) = O(N^{-1} \ln^p \frac{N}{2})$. So, as Figure 3 (right) demonstrates, the error of order (almost) 1 becomes spread throughout the boundary-layer region. Consequently, when the errors are computed in the L_2 norm, Triangulation B is superior to C (as shown in Table 4).

The computational convergence rates in Table 4 can be explained by a similar, but more detailed error analysis. To be more precise, with the notation $\mathcal{E}_s := (N^{-1} \ln^p \frac{N}{2})^s e^{-Cx/\varepsilon}$, it suffices to show that the error $|[U-u](x, \frac{j}{M})|$ roughly

behaves like $\mathcal{E}_2$ for Triangulation A, and like $\mathcal{E}_1$ for Triangulation C, while for Triangulation B it behaves like $\mathcal{E}_1$ when $j = \frac{M}{2}$ and like $\mathcal{E}_2$ otherwise.

3.2. **Standard Linear Finite Elements.**

Lemma 3.7 (Non-lumped-mass case)**.** *The statement of Lemma 3.3 remains valid for the computed solution U obtained using standard linear finite elements.*

Proof. We imitate the proof of Lemma 3.3 with a few changes described below.

(i) This part of the proof is devoted to establishing (3.5), only now $\mathring{U}(x_i,0)$ satisfies (3.3), i.e. $\tilde{\mathcal{L}}^h\mathring{U}(x_i,0) = 0$ for $i = 1,\dots,2N_0-1$. So a version of (3.6) for for $e := \mathring{U} - u$ is obtained using the definition of $\tilde{\mathcal{L}}^h$ in (3.3) and the structure of the mesh (see Figure 2):

$$\tilde{\mathcal{L}}^h e(x_i,0) = \tilde{L}_x^h e_i := \tfrac{\varepsilon^2}{h^2}\big(1-\tfrac{h^2}{12\varepsilon^2}\big)\big[-e_{i-1}+2e_i-e_{i+1}\big] + \big[\tilde{\gamma}_i + \tfrac{2\varepsilon^2}{H^2}\big]e_i. \tag{3.10}$$

Here $\tilde{\gamma}_i := \gamma_i - \frac{4}{12} = \frac{2}{3}$ for $i \neq N_0$ and $\tilde{\gamma}_{N_0} := \gamma_{N_0} - \frac{2}{12} = \frac{1}{2}$, while $\frac{h}{\varepsilon} = N_0^{-1}$ is assumed sufficiently small, so the one-dimensional discrete operator $\tilde{L}_x^h$ satisfies the discrete maximum principle and is handled similarly to L_x^h of (3.6).

Next, by virtue of $\tilde{\mathcal{L}}^h e(x_i,0) = -\tilde{\mathcal{L}}^h u(x_i,0)$, a version of (3.7) is given by

$$\tilde{\mathcal{L}}^h e(x_i,0) = [\mathcal{L}^h - \tilde{\mathcal{L}}^h]u(x_i,0) + [1-\gamma_i]\,u(x_i,0) + \mathcal{O}\big(\tfrac{h^2}{\varepsilon^2}\big). \tag{3.11}$$

Note that the definition of $\tilde{\mathcal{L}}^h$ in (3.3) implies that

$$[\mathcal{L}^h - \tilde{\mathcal{L}}^h]u(x_i,0) = \tfrac{1}{12}\sum_{(x',y')\in\mathcal{S}_i}[u(x_i,0) - u(x',y')],$$

where $\mathcal{S}_i$ is the set of meshnodes that have a common edge with $(x_i,0)$. The right-hand side here involves $u(x',\pm H) = u(x',0)$, so, with the notation $u_i := u(x_i,0)$, a calculation using the structure of the mesh (see Figure 2) yields

$$[\mathcal{L}^h - \tilde{\mathcal{L}}^h]u(x_i,0) = \tfrac{1}{12}\big[-u_{i-1}+2u_i-u_{i+1}\big] + \tfrac{1}{12}F_i = \mathcal{O}\big(\tfrac{h^2}{\varepsilon^2}\big) + \tfrac{1}{12}F_i, \tag{3.12}$$

where

$$F_i := \hat{\alpha}_i(u_i-u_{i+1}) + \check{\alpha}_i(u_i-u_{i-1}), \quad \hat{\alpha}_i := \begin{cases} 2, & i < N_0 \\ 0, & i \geq N_0 \end{cases}, \quad \check{\alpha}_i := \begin{cases} 0, & i \leq N_0 \\ 2, & i > N_0 \end{cases}.$$

Next, define a decomposition $F_i = F_i' + F_i''$ with

$$F_i' := \begin{cases} -F_{2N_0-i}, & i \leq N_0 \\ F_i, & i \geq N_0 \end{cases} \Rightarrow\ F_i'' = \hat{\alpha}_i\big[(u_i-u_{i+1}) + (u_{2N_0-i} - u_{2N_0-i-1})\big].$$

Here, by virtue of $u_j = e^{-x_j/\varepsilon}$, one has $u_j - u_{j+1} = u_j(1-e^{-h/\varepsilon})$ for any j, so one can easily check that $F_i'' \geq 0$. Combining this with (3.10), (3.11) and (3.12) yields

$$\tilde{L}_x^h e_i = \tilde{\mathcal{L}}^h e(x_i,0) \geq \tfrac{1}{12}F_i' + [1-\gamma_i]\,u(x_i,0) + \mathcal{O}\big(\tfrac{h^2}{\varepsilon^2}\big).$$

To deal with F_i', let $\tilde{L}_x^h e_i' = \frac{1}{12}F_i'$ subject to $e_0' = e_{2N_0}' = 0$. The symmetry of this problem combined with the symmetry of F_i' immediately implies that $e_{N_0}' = 0$. Now $\tilde{L}_x^h[e_i - e_i'] \geq [1-\gamma_i]\,u(x_i,0) + \mathcal{O}\big(\frac{h^2}{\varepsilon^2}\big)$ yields a version of (3.5) for this equation $e_{N_0} - e_{N_0}' \geq 2C_0N_0^{-1}$ (with a different C_0). As $e_{N_0}' = 0$, the desired bound (3.5) follows.

(ii) This part of the proof is identical with part (ii) in the proof of Lemma 3.3. To show that $|Z|$ attains its maximum on $\partial\mathring{\Omega}$, move the terms $Z_i^{\pm}$, available from the boundary data, to the right-hand side in the discrete equation $\tilde{\mathcal{L}}^h Z = 0$. The

resulting nonhomogeneous one-dimensional discrete equation for the unknown vector $\{Z_i\}_{i=0}^{2N_0}$ satisfies the discrete maximum principle, which can be used to deduce that the maximum of $|Z|$ indeed occurs on $\partial\mathring{\Omega}$. □

References

[1] V. B. Andreev, *The logarithmic factor in the L_∞-norm error estimate for linear finite elements is sharp*, Semin. I. Vekua Inst. Appl. Math. Rep. (Dokl. Semin. Inst. Prikl. Mat. im. I. N. Vekua), 4 (1989), no. 3, 17–20 (in Russian).

[2] N. S. Bakhvalov, On the optimization of methods for solving boundary value problems with boundary layers, Zh. Vychisl. Mat. Mat. Fis., 9 (1969), 841–859 (in Russian).

[3] H. Blum, Q. Lin and R. Rannacher, *Asymptotic error expansion and Richardson extrapolation for linear finite elements*, Numer. Math. 49 (1986), 11–37.

[4] L. Chen, P. Sun, J. Xu, *Optimal anisotropic meshes for minimizing interpolation errors in L^p-norm*, Math. Comp. 76 (2007), 179–204.

[5] C. Clavero, J. L. Gracia and E. O'Riordan, *A parameter robust numerical method for a two dimensional reaction-diffusion problem*, Math. Comp., 74 (2005), 1743–1758.

[6] E. F. D'Azevedo, *Optimal triangular mesh generation by coordinate transformation*, SIAM J. Sci. Statist. Comput., 12 (1991), 755–786.

[7] E. F. D'Azevedo and R. B. Simpson, *On optimal interpolation triangle incidences*, SIAM J. Sci. Statist. Comput., 10 (1989), 1063–1075.

[8] V. Dolejší, J. Felcman, *Anisotropic mesh adaptation for numerical solution of boundary value problems*, Numer. Methods Partial Differential Equations, 20 (2004), 576–608.

[9] N. Kopteva, *Maximum norm error analysis of a 2d singularly perturbed semilinear reaction-diffusion problem*, Math. Comp., 76 (2007), 631–646.

[10] H.-G. Roos, M. Stynes and L. Tobiska, *Robust Numerical Methods for Singularly Perturbed Differential Equations*, Springer, Berlin, 2008.

[11] A. A. Samarskii, *Theory of difference schemes*, Nauka, Moscow, 1989 (Russian), translation in A. A. Samarskii, *The theory of difference schemes*, Marcel Dekker, New York, 2001.

[12] A. H. Schatz and L. B. Wahlbin, *On the quasi-optimality in L_∞ of the $\mathring{H}^1$-projection into finite element spaces*, Math. Comp. 38 (1982), 1–22.

[13] A. H. Schatz and L. B. Wahlbin, *On the finite element method for singularly perturbed reaction-diffusion problems in two and one dimensions*, Math. Comp., 40 (1983), 47–89.

[14] G. I. Shishkin, *Grid approximation of singularly perturbed elliptic and parabolic equations*, Ur. O. Ran, Ekaterinburg, 1992 (in Russian).

Department of Mathematics and Statistics, University of Limerick, Limerick, Ireland
E-mail address: natalia.kopteva@ul.ie